Received: 22 March 2025 | Accepted: 10 June 2025

DOI: 10.1111/jpy.70079

RESEARCH ARTICLE

The effects of iron limitation on the small chlorophyte *Micromonas* from the Northeast Pacific Ocean

Meredith G. Meyer | **Vincent J. White** | **Olivia Torano** | **Heidi Hannoush** | **Margarita Lankford** | **Adrian Marchetti**

Department of Earth, Marine, and Environmental Sciences, University of North Carolina at Chapel Hill, Chapel Hill, North Carolina, USA

Correspondence
Adrian Marchetti, Department of Earth, Marine, and Environmental Sciences, University of North Carolina at Chapel Hill, Chapel Hill, NC, USA.
Email: amarchetti@unc.edu

Funding information
Biological and Physical Sciences Division, Grant/Award Number: 80NSSC17K0552; Division of Ocean Sciences, Grant/Award Number: OCE2219973

Editor: B. Palenik

Abstract

Small eukaryotic phytoplankton can account for a considerable amount of biomass and primary production in high nutrient, low chlorophyll (HNLC) regions of the ocean where iron limitation is pronounced. However, the physiological and metabolic strategies these cells invoke to cope under low iron conditions and the extent to which they are responsible for new production (i.e., the fraction of primary production supported by nutrients from outside of the euphotic zone) are unclear. Here, we examined how a representative picoeukaryote—the chlorophyte *Micromonas* sp., recently isolated from the iron-limited subarctic Northeast Pacific Ocean—responded to iron limitation when grown on nitrate as a nitrogen source. Iron-limited *Micromonas* exhibited reductions in growth rate, cell volume, and elemental quotas along with a restructuring of cellular metabolism. Gene expression and metabolic pathway analyses showed evidence of strategies to mitigate iron limitation with constitutive expression of genes related to nitrogen uptake and utilization. Additionally, cellular carbon and nitrogen quotas were 20–70 fmol C · cell^{-1} and 3.3–20 fmol N · cell^{-1}, respectively, as a function of iron status. Based on the measured cellular quotas, we have estimated that representative picoeukaryotes (<2 μm), such as *Micromonas,* in HNLC Northeast Pacific waters can account for a significant proportion of new production, supporting the need for a reconsideration of the role small eukaryotic phytoplankton play in the global carbon cycle.

KEYWORDS
iron limitation, nitrogen, picoeukaryotes, primary production

INTRODUCTION

In open-ocean ecosystems, high surface-area-to-volume ratios and generally lower nutrient quotas make picophytoplankton strong competitors for nutrients, thus enabling them to routinely dominate eukaryotic phytoplankton communities in these oligotrophic environments (Worden & Not, 2008). Although much research has focused on cyanobacteria, specifically *Prochlorococcus* (Chisholm et al., 1991) and *Synechococcus* (Moore et al., 2002), fewer studies have investigated the growth strategies of picoeukaryotes that have been shown to potentially play key biogeochemical roles (Fowler et al., 2020). Previous studies have suggested

Abbreviations: *AMT*, ammonium transporters; Chl *a*, chlorophyll *a*; CPM, counts per million; EDTA, ethylenediamine tetraacetic acid; EXPORTS, The NASA EXport Processes in the Ocean from RemoTe Sensing Program; HNLC, high nutrient, low chlorophyll; ISIP, iron starvation induced proteins; KEGG, Kyoto Encyclopedia of Genes and Genomes; KO, KEGG ortholog; NCBI, National Center for Biotechnical Information; NH_4^+, ammonium; *NiR*, nitrite reductase; NO_3^-, nitrate; *NR*, nitrate reductase; *NRT*, nitrate/nitrite transporters; PC, particulate carbon; pCO_2, partial pressure of carbon dioxide; PN, particulate nitrogen; *Psa*, photosystems I; *Psb*, photosystems II; PSII, photosystem II; RFUs, relative fluorescent units; Station P, Ocean Station Papa; *Urt*, urea transporters; μ, growth rate; μ_{max}, maximum growth rate; σ_{PSII}, cross-sectional absorption area of photosystem II.

chlorophytes and other small eukaryotic groups primarily rely on ammonium and other forms of recycled nitrogen to support their growth (Greene et al., 1992; Marchetti et al., 2006; Meyer et al., 2022). Compared to cyanobacteria, diatoms, and dinoflagellates, these picoeukaryotes have been poorly characterized and are less likely to be available in culture. Thus, there are fewer monocultured representatives sequenced for genomic and/or transcriptomic analyses compared to other phytoplankton groups (Le Gall et al., 2008). This overall lack of knowledge has led to these organisms commonly being overlooked in whole-community analyses despite their high abundances.

Given the potentially outsized role these eukaryotic picophytoplankton could play in oligotrophic and nutrient-limited regions, understanding the nutrient acquisition strategies, requirements, and metabolisms employed by these phytoplankton and the resultant effects on general ecosystem productivity and carbon export potential is of substantial importance. Here we have presented measurements obtained from the chlorophyte *Micromonas* sp., which was recently isolated from Ocean Station Papa (Station P) in the subarctic Northeast Pacific during the NASA EXport Processes in the Ocean from RemoTe Sensing (EXPORTS) program in 2018. *Micromonas* sp. is an abundant member of the Mamiellales order and is closely related to *Ostreococcus* and *Bathycoccus* (Monier et al., 2016; Vannier et al., 2016), two other ecologically important picoeukaryotic chlorophytes. Studies have shown that *Micromonas* can occupy a wide range of habitats, from the tropics to the poles as well as offshore and coastal environments (Demory et al., 2019). The group often exhibits an "occupancy-abundance relationship" wherein *Micromonas* and other members of the *Mamiellophyceae* lineage frequently become the most abundant genera in regions where they have the largest range (Monier et al., 2016, p. 464). Yet, the metabolic capabilities and the ecological role of *Micromonas* in iron-limited regions is still poorly understood.

Station P is the site of a long-term oceanographic monitoring program that resides within a high nutrient (predominantly nitrate, NO_3^-), low chlorophyll (or HNLC) region. This region is chronically limited by the bioavailability of iron, which, despite replete macronutrient concentrations, inhibits substantial phytoplankton biomass standing stock and higher rates of primary production (Marchetti et al., 2006; Martin & Fitzwater, 1988). Iron is crucial as a co-factor in photosynthesis and nitrogen assimilation (La Roche et al., 1993; Peers & Price, 2006). Many groups of phytoplankton that experience iron limitation have been shown to utilize regenerated nitrogen sources (e.g., ammonium, NH_4^+, or urea) which theoretically have lower iron requirements relative to oxidized forms of nitrogen or nitrogen gas (Price et al., 1994; Varela & Harrison, 1999). In addition, recent findings have suggested that the most dominant ecotype of the cyanobacteria in the Northeast Pacific, *Synechococcus*, lacks the ability to assimilate NO_3^-, thus being restricted to regenerated production (i.e., using recycled nitrogen sources such as ammonium and urea; Sharpe et al., 2023). This finding introduces a knowledge gap in our understanding of which organisms are responsible for the vast majority of new production in the region, which has routinely been measured to be driven predominantly by small phytoplankton groups (i.e., <5 μm in cell diameter; Meyer et al., 2022).

Here, we sought to examine why *Micromonas* abundance is high in the Northeast Pacific and what their possible role is in carbon export. We had two primary research objectives: (a) examine the distinct physiological and metabolic strategies of *Micromonas* grown under low iron conditions and (b) quantify the extent to which *Micromonas* can contribute substantially to new production in this region. We pursued these objectives by determining rates of cellular growth, photophysiology, carbon and nitrogen cellular content, and trends in gene expression as a function of iron status. The combination of molecular and physiological analyses provides a more holistic approach to examining ecologically important phytoplankton groups and their influence on marine biogeochemical cycles.

MATERIALS AND METHODS

Sampling and cell isolation

Whole seawater was collected from approximately 5 m depth via a trace metal clean rosette during the NASA EXPORTS field campaign to Station P in the subarctic North Pacific. This campaign occurred from August 16 to September 7, 2018. To keep storage conditions as similar to the ambient environment as possible, sampled seawater was placed in culture flasks and incubated in on-deck incubators before being transported back to the University of North Carolina for phytoplankton isolation. An abundant, small (<5 μm) chlorophyte was isolated via single-cell isolation using a 10-μL pipette. DNA was extracted using standard protocols with a DNEasy Plant Mini Kit (Qiagen). The V4 region of the 18S rRNA gene was sequenced (National Center for Biotechnology Information, NCBI, accession number SAMN47284909), and the consensus sequence of forward and reverse reads was searched against the NCBI repository using BLAST, revealing the highest sequence similarity to *Micromonas pusilla* (accession number KY980282.1) with a 100% ID and 76% query cover.

Culture conditions

Micromonas sp. (UNC1837) cells were maintained in Aquil media in an incubator under constant 120–150 μmol photons $\cdot m^{-2} \cdot s^{-1}$ light at 12°C to maintain

light saturation and ambient temperatures close to the environmental conditions at Station P. To examine the effects of differing nitrogen (N) forms under variable iron (Fe) states on *Micromonas* growth and physiology, four trace-metal-clean culture treatments were initiated. Aquil medium was sterilized in a microwave, cooled, and supplemented with filter-sterilized (0.2-μm Acrodisc) ethylenediamine tetraacetic acid (EDTA) trace metals (minus iron), vitamins (B_{12}, thiamine, and biotin), and chelexed macronutrients (phosphate and NO_3^- or NH_4^+, depending on treatment) in accordance with Aquil medium concentrations (Price et al., 1989). Trace-metal concentrations were buffered using 100 μM of EDTA. Two treatments contained NO_3^- (300 μM), and two treatments contained NH_4^+ (30 μM) as their nitrogen source. Within each nitrogen treatment, there was an iron-replete (1370 nM total Fe) and an iron-deplete (3.1 nM total Fe) treatment. Iron concentrations were selected after initial testing, and the chosen concentrations were able to achieve the most consistent growth rates after a minimum of three transfers, with transfers occurring approximately every 7–10 days. Thus, the four treatments can be described as NO_3^- Fe+, NO_3^- Fe–, NH_4^+ Fe+, and NH_4^+ Fe–. Each treatment was first cultured in triplicate acid-washed, 28-mL, clear polycarbonate centrifuge tubes (Nalgene, Rochester, New York) for acclimation to their respective treatments. Cells were acclimated to their treatment for a minimum of three transfers before experiments began. During acclimation, 200 μL of dense late-exponential-phase culture was transferred to new tubes with fresh media to maintain growth, thus representing a 125-fold dilution. Following acclimation, cultures were transferred to a trace-metal-clean, 1-L polycarbonate bottle that was approximately 700 mL full. We were not able to maintain steady-state growth rates in the NH_4^+ Fe+ and NH_4^+ Fe– cultures, thus confining our experiment to the NO_3^- Fe+ and NO_3^- Fe–, referred to as Fe+ and Fe– treatments herein. All culture preparation, maintenance, and cell transfers were conducted in a trace-metal-clean room under a positive-pressure, laminar flow hood.

During the experiments, approximate cell growth rates and concentrations were monitored via relative fluorescence units (RFUs) on a Turner 10 AU fluorometer from lag phase through stationary phase (Brand et al., 1981). Once samples were determined to be in mid-exponential phase, cultures were measured for RFUs and other photophysiological parameters using a Satlantic FIRe fluorometer with a blue light diode (450 nm) and 60 iterations per triplicate measurement (see below) and harvested for the following parameters: cell counts, chlorophyll *a* (Chl *a*) concentration, particulate carbon (PC) and nitrogen (PN) concentration, and RNA.

Specific growth rates (μ) were calculated as the slope of the natural log of relative fluorescence units over time, according to Brand et al. (1981). Assuming Fe+ represented a maximum growth rate (μ_{max}), the ratio of average μ/μ_{max} (i.e., Fe–/Fe+) was calculated. The maximum quantum yield of photochemistry in photosystem II (PSII; F_v/F_m) and the functional absorption cross section of PSII (σ_{PSII}) were measured as metrics to evaluate photosynthetic efficiency (Gorbunov & Falkowski, 2004).

Chlorophyll *a* was analyzed fluorometrically following Graff and Rynearson (2011). Particulate carbon (PC) and particulate nitrogen (PN) were analyzed on a Carlo Erba NC 2500 elemental analyzer at the University of Maryland Center for Environmental Science Appalachian Laboratory in Frostburg, Maryland. Cultures for RNA were filtered onto an Isopore 0.4-μm pore size, 47-mm polycarbonate filter under gentle vacuum pressure, flash frozen in liquid nitrogen, and stored at −80°C before extraction. RNA was extracted using standard protocols with a RNAqueous-4PCR kit according to the manufacturer's protocols. Extracted RNA was checked for quality (A280/260, A260/230, and nucleic acid concentration) on a Nanodrop spectrophotometer and cleaned using a RNeasy MinElute Clean-up kit. RNA was sent to the Azenta Genewiz Sequencing Facility in South Plainfield, New Jersey for Illumina high throughput analysis with ~350 M raw paired-end reads per lane and single index, 2 × 150 bp per lane, resulting in a read depth of 62–65 million reads per sample.

Cell counts and size estimates

A small aliquot (1.8 mL) of each culture (both treatments and all replicates) was preserved in 200 μL of paraformaldehyde in 2-mL cryovials at the time of cell harvest, the day following the harvest, and several (2–3) days preceding the harvest. Cryovials were flash frozen in liquid nitrogen and stored at −80°C until they were analyzed on a Guava easyCyte flow cytometer equipped with a red laser in the Paerl Lab at North Carolina State University. Data were processed by InCyte software to provide cell counts based on red fluorescence (Figure S1). Estimates of cell size (diameter) were also calculated using calibration beads of known size based on the relationships of Paerl et al. (2020). Cell volume was calculated by assuming cells were spherical. Cellular Chl *a* and PC and PN concentrations were calculated by normalizing concentrations by cell counts and by cell biovolume.

North Pacific new production calculations

Assuming *Micromonas* is a good representative (i.e., in the top 20% most represented species in 18S rRNA gene community composition data; Jones & Rynearson, 2022) of the picoeukaryote population at

Station P, the upper bound estimates of the contribution of picoeukaryotes to total new production under Fe-replete and Fe-limiting conditions were calculated according to Equation 1:

$$\text{New production} = \text{cell concentration} \times \mu \times \text{N quota} \quad (1)$$

where the nitrogen quota is in units of fmol N · cell^{-1}. In the equation, the N quota and growth rate (μ; d^{-1}) came from our laboratory results with the *Micromonas* culture. The cell concentration used in Fe+ and Fe− culture new production rates was the picoeukaryote cell counts (mean of 3.3×10^6 cells · L^{-1}) measured from the EXPORTS Northeast Pacific cruise in 2018 (Graff, 2023). These were average picoeukaryote counts collected from surface waters and measured via flow cytometry during the observation period.

Gene expression analysis

Transcripts were trimmed of sequence adapters and poly-A tails via Trim_galore (v.0.6.2; Altos Labs) and underwent quality control analysis via FastQC (v.0.11.9) via which sequences with a quality score below 20 and/or a length less than 50 bp were removed. Merged sequence files were assembled de novo via Trinity (v.2.8.6) before being combined into grand assemblies based on iron treatment via cdhit (v.4.8.1; Fu et al., 2012). Sequences underwent functional annotation via the Kyoto Encyclopedia of Genes and Genomes (KEGG; Release 88.2). Additional manual annotation of genes associated with Fe metabolism, but which were not included in KEGG (e.g., proton-pumping rhodopsins; iron starvation-induced proteins, ISIPs; and phytotransferrins), was conducted (see Moreno et al., 2017 for more information on manual annotation and sequence acquisition). Independent end-to-end read alignment occurred via Salmon (v.10.9.1; Patro et al., 2017), and annotation and count files were combined via tximport, providing counts per million (CPM) values per gene per sample (Soneson et al., 2015). Differential expression of genes was analyzed at the KEGG ortholog (KO) level, averaging values for multiple contigs with the same KO, according to the DESeq2 package in RStudio (v.4.2.2). The Log2Fold change (adjusted p-value < 0.05) of specific genes of interest, particularly those associated with photosynthesis, N metabolism, and Fe metabolism, were investigated. Additionally, trends in KEGG metabolic pathways were analyzed among samples. Figures were generated in Matlab R2022b. Sequences from this analysis are available at NCBI (accession numbers: SAMN39858273-284). Further details on bioinformatic processing and visualization are available in Figure S2.

RESULTS

Growth rates and photosynthetic efficiency

The Fe+ cultures had an average growth rate of $0.96 \pm 0.01 \cdot$ d^{-1} (Figure 1a). The average growth rate of Fe− cultures was substantially lower at $0.48 \pm 0.07 \cdot$ d^{-1} resulting in a μ/μ_{max} (Fe−/Fe+) of 0.50, suggesting substantial limitation of iron in the Fe− treatment relative to the Fe+ treatment (Figure 1a). Estimates of maximum photochemical yield of PSII (F_v/F_m) confirmed that the Fe+ cultures had an increased efficiency of PSII compared to Fe−, which experienced iron-limited conditions. The mean F_v/F_m for the Fe+ treatment was 0.73 ± 0.02, whereas values for the Fe− cultures were 0.37 ± 0.03, consistent with a decline in photosynthetic efficiency of PSII due to iron limitation (Figure 1b). The cross-sectional absorption area of photosystem II (σ_{PSII}) was also consistent with other iron-limited phytoplankton cultures with an increase in σ_{PSII} under iron-limited conditions (Ellis, 2015; Moreno et al., 2020). For Fe− cultures, σ_{PSII} averaged 1036 ± 264, and for Fe+, σ_{PSII} averaged 372 ± 12 (data not shown), resulting in a 2.8-fold increase under iron-limited conditions.

There was a substantially lower F_v/F_m value for the Fe+ replicate A sample compared to the other replicates, suggesting that this culture may have entered stationary phase and was experiencing N depletion at the time of sampling. This triplicate was therefore removed from the averages of Fe+ sample data presented in Figures 1 and 2 as well as from the gene expression analysis; however, with all replicates included, there was still a significant difference in growth rates, cellular Chl *a* concentrations, and cellular C and N quotas between the Fe+ and Fe− treatments (Table S1).

Cell size and chlorophyll *a* content

The Fe+ cultures had an average cell diameter of $1.85 \pm 0.02\,\mu$m (data not shown) and corresponding cell volume of $3.35 \pm 0.10\,\mu$m^3 (Figure 1c). The Fe− cultures had an average cell diameter of $1.58 \pm 0.00\,\mu$m and cell volume of $2.07 \pm 0.00\,\mu$m^3 (Figure 1c).

Cellular Chl *a* contents exhibited an order of magnitude difference between the Fe+ and Fe− samples, with the Fe+ cultures having an average of 6.42 ± 0.50 fg · cell^{-1} and the Fe− cultures averaging only 0.53 ± 0.09 fg · cell^{-1}. Chlorophyll *a* concentration, when normalized to cell biovolume, exhibited a similar trend to cellular Chl *a* content, but the difference in the magnitude between the Fe+ and Fe− cultures was substantially lower (Figure 1d). The average biovolume-normalized Chl *a* content was 1.92 ± 0.09 fg · μm^{-3} in the Fe+ treatment and 7.5-fold lower at 0.25 ± 0.04 fg · μm^{-3} in the Fe− treatment.

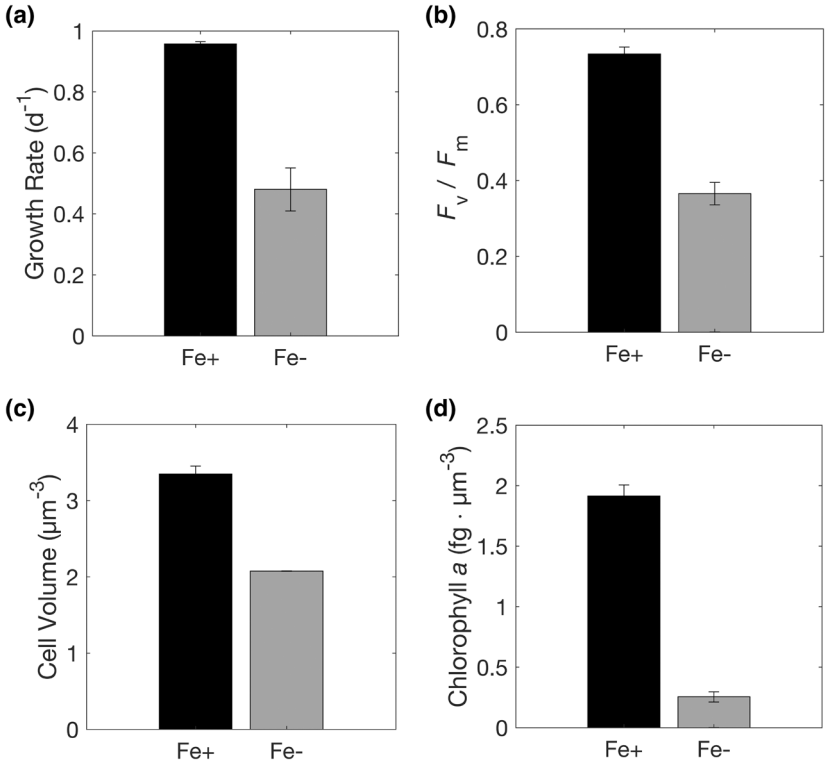

FIGURE 1 Specific growth rates (a; d^{-1}), maximum photochemical efficiencies of PSII (b; F_v/F_m), cell volumes (c; μm^3), and cellular chlorophyll *a* quotas (d; fg · μm^{-3}) for *Micromonas* grown under iron-replete (Fe+) and iron-limited (Fe–) conditions. Error bars represent standard deviations with $n = 3$ for Fe– and $n = 2$ for Fe+.

Cellular carbon and nitrogen quotas

Like Chl *a*, the cellular carbon (C) content exhibited an order of magnitude difference between the Fe+ and Fe– treatments. The Fe+ cultures had a high cellular C quota of 158 ± 20 fmol C · cell^{-1} whereas the Fe– cultures had an eight-fold lower C quota of 23 ± 0.0 fmol C · cell^{-1} (Figure 2a). As is seen throughout the parameters measured, the Fe– sample quotas were consistent, only ranging from 22 to 24 fmol C · cell^{-1} among triplicates. When normalized to cell volume, the biovolume-normalized C quotas were more similar between treatments due to the cells in the Fe+ culture being ~1.5-fold larger than the cells in the Fe– culture. The Fe+ treatment had a C quota of 47 ± 3.8 fmol C · μm^{-3} whereas the quota for the Fe– treatment was 11.1 ± 0.38 fmol C · μm^{-3} (Figure 2b). Thus, when considering the difference in cell volumes (i.e., calculated per μm^{-3} rather than per cell), the difference in C quota decreased from 8.0- to 4.3-fold higher in the Fe+ treatment relative to the Fe– treatment.

The cellular N contents likewise exhibited orders of magnitude differences between iron treatments when normalized per cell and per unit volume. The average N quota for the Fe+ cultures was 21.1 ± 1.5 fmol N · cell^{-1} whereas the average for the Fe– cultures was 3.37 ± 0.13 fmol N · cell^{-1} (Figure 2c). The per unit volume average for Fe+ samples was 6.30 ± 0.26 fmol N · μm^{-3} and for the Fe– samples was $1.62 \pm 6.44 \times 10^{-2}$ fmol N · μm^{-3} (Figure 2d). The change in cellular N contents as a function of iron status was similar to that of C at approximately six- and four-fold larger for the Fe+ treatment when normalized per cell and per unit volume, respectively. Both treatments exhibited slightly higher particulate carbon:nitrogen (C:N) ratios than the Redfield ratio of 6.6 with averages of 7.49 ± 0.30 and 6.84 ± 0.05 for Fe+ and Fe–, respectively (Figure 2e). The C:Chl *a* ratios exhibited the opposite pattern with a higher average ratio (537 ± 111) in the Fe– treatment than in the Fe+ treatment (296 ± 9.74; Figure 2f).

Potential contributions to new production in the NE Pacific

Picoeukaryote cell concentrations during the EXPORTS observation period used in these calculations ranged between 2.14×10^6 and 5.05×10^6 cells · L^{-1} (Graff, 2023). Based on these picoeukaryote cell densities, rates of potential contributions to new production varied by an order of magnitude between iron treatments, ranging from 3.7 to 8.4 nmol N · L^{-1} · d^{-1} (average of 5.4 ± 1.0 nmol N · L^{-1} · d^{-1}) for Fe-limited cells and 45.9 to 105.1 nmol N · L^{-1} · d^{-1} (average of 67.5 ± 4.3 nmol N · L^{-1} · d^{-1}) for Fe-replete cells

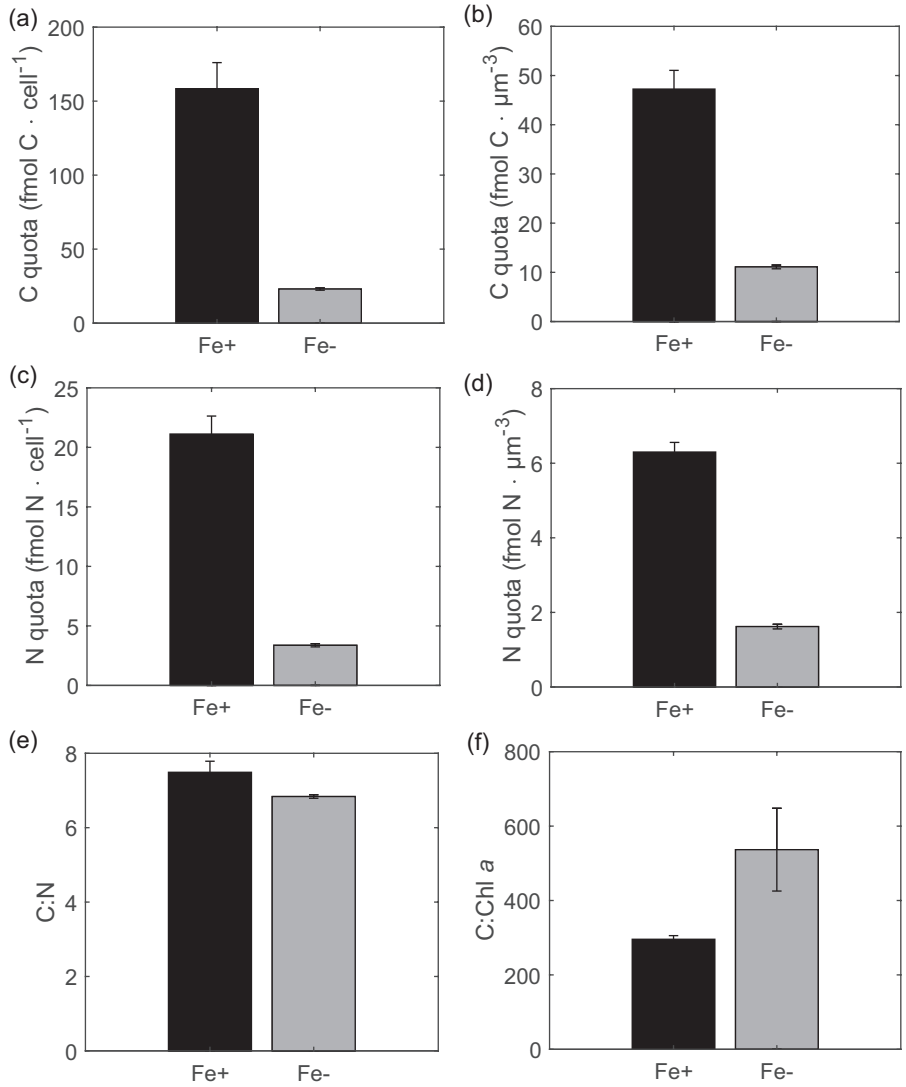

FIGURE 2 Cellular carbon (a, b) and nitrogen (c, d) quotas and C:N (e) and C:Chl *a* (f) ratios for *Micromonas* grown under iron-replete (Fe+) and iron-limited (Fe–) conditions. Quotas are represented per cell (a, c; fmol · cell^{-1}) and per cell volume (b, d; fmol · µm^{-3}). Error bars represent standard deviations with $n = 3$ Fe– and $n = 2$ for Fe+.

(Figure 3). The rates of small-celled new production at Station P were generally between these lower and upper limits based on iron status, except for on day 240 of the year, when the EXPORTS rate was higher.

Gene expression

Molecular sequencing of the *Micromonas* sp. (UNC1837) transcriptome indicated a higher GC content for the Fe+ (61%) versus Fe– (49%) cultures. Total sequences and sequence length were comparable between treatments for the Fe+ and Fe–, respectively.

The impact of Fe availability was analyzed broadly on the metabolic pathway level (Figure 4a) and, specifically, on a targeted gene level (Figure 4b). Of the 17 metabolic pathways of interest analyzed, on average 10 displayed overrepresentation in Fe– treatment (i.e., negative Log2Fold change). Key pathways exhibiting this trend included those related to iron-limitation mitigation strategies or general physiological stress responses, including iron starvation induced protein 3 (ISIP3) expression, ferredoxin expression, higher expression of photosystem I relative to photosystem II, and zeaxanthin epoxidase (Figure 4a). Unsurprisingly, many gene transcripts involved in pathways related to general cell maintenance, including nitrogen metabolism, arginase, flavin adenine dinucleotide synthesis, etc., were overrepresented in the Fe+ treatment.

Evaluating these physiological trends further, our results appeared consistent with those previously reported for the closely-related chlorophyte *Ostreococcus* (Lelandais et al., 2016), with *Micromonas* appearing to contain far fewer transcribed

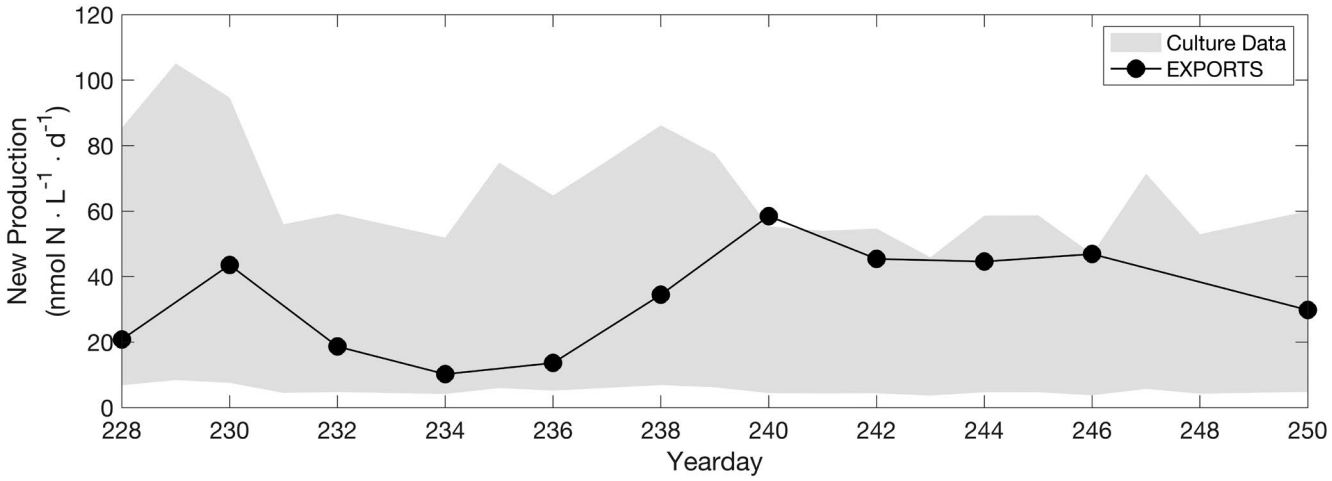

FIGURE 3 Estimates of *Micromonas* sp. contributions to new production during the North Pacific EXPORTS cruise. *Micromonas* sp. new production rate estimates for NO_3^- Fe− and NO_3^- Fe+, are calculated from culture-based growth rates, cellular N quotas, and in situ NP EXPORTS picoeukaryotic cell counts obtained from flow cytometry. The gray shaded region represents the upper bounds (NO_3^- Fe+) and lower bounds (NO_3^- Fe−) for the culture-based rate estimates (labeled as Culture Data). The black line represents the average mixed-layer rates of new production of the small the size-fraction (<5 μm) during EXPORTS by day of the year during the observation period.

genes involved in nitrogen and iron metabolism than have been commonly reported in diatoms and other phytoplankton taxa. Transcripts for the nitrogen assimilation genes nitrate/nitrite transporters (*NRT*), nitrate reductase (*NR*), nitrite reductase (*NiR*), ammonium transporters (*AMT*), and urea transporters (*Urt*) were identified in our *Micromonas* isolate (Figure 4b,c). Most genes associated with NO_3^- uptake (*NRT* and *NiR*) increased expression (Log2Fold changes >0) in the Fe+ treatment relative to Fe− treatment (Figure 4b). Urea transporters were also overrepresented (Log2Fold change = 4.21; adjusted *p*-value < 0.01) under Fe+ conditions. Conversely, ammonium transporters showed a slight negative Log2Fold change (−0.47), suggesting increased expression in the Fe− treatment (Figure 4b,c). Overall, genes associated with the expression of photosystems I and II (*Psa* and *Psb*) exhibited a stronger Log2Fold change (−2.93) in Fe− conditions, which was in contrast to the common assumption that these photosynthetic genes should be more highly expressed under iron-replete conditions (Figure 4b).

Our data suggest that *Micromonas* may lack genes commonly involved in iron regulation and homeostasis in diatoms residing in HNLC regions, including proton-pumping rhodopsins and ferritin (Andrew et al., 2023; Marchetti et al., 2009). However, we did identify that the gene for iron starvation induced protein 3 (*ISIP3*), which was strongly expressed (Log2Fold change = −4.62; adjusted *p*-value < 0.01) under Fe− conditions (Figure 4b). The percent of overall contigs without a functional annotation was high (87.9%), suggesting additional genes involved in both nitrogen and iron metabolism may have been present but were not readily identified in the KEGG database.

DISCUSSION

Cellular and metabolic characterization

Although less is known about the ecology and physiology of *Micromonas* relative to other picoeukaryotic chlorophytes such as *Ostreoccocus*, our results were consistent with and can build upon some of what has been reported on *Micromonas* (Cochlan & Harrison, 1991a, 1991b). Our estimates of cell size were similar to the previously reported values of <2 μm (McKie-Krisberg & Sanders, 2014). Additionally, *Ostreoccocus* has been reported to exhibit fast growth rates under nitrogen replete conditions (μ_{max} of 1.11 · d^{-1}; Cochlan & Harrison, 1991a), consistent with our measured growth rates for our *Micromonas* sp. isolate in iron-replete conditions. Additionally, our inability to achieve steady state growth in our isolate using NH_4^+ media is noteworthy. In fact, following nitrogen starvation, Cochlan and Harrison (1991a, 1991b) reported *M. pusilla* had a preference for NH_4^+ and urea uptake relative to NO_3^- uptake. Although we were unable to identify what was inhibiting growth, it is likely that our *Micromonas* sp. required specific conditions for NH_4^+ utilization that were not met within our culture conditions. Our results suggest that our strain of *Micromonas* may exhibit a preference for NO_3^- over other forms of nitrogen (such as NH_4^+), but further research is warranted.

Our study quantified changes in cellular Chl *a* concentration and C and N quotas in iron-replete and iron-deplete *Micromonas* sp. cells. Understanding these iron-limitation-driven differences is critical, as changes in growth rates and elemental quotas of *Micromonas* may have ecosystem and biogeochemical implications in HNLC regions. Consistent with current paradigms of

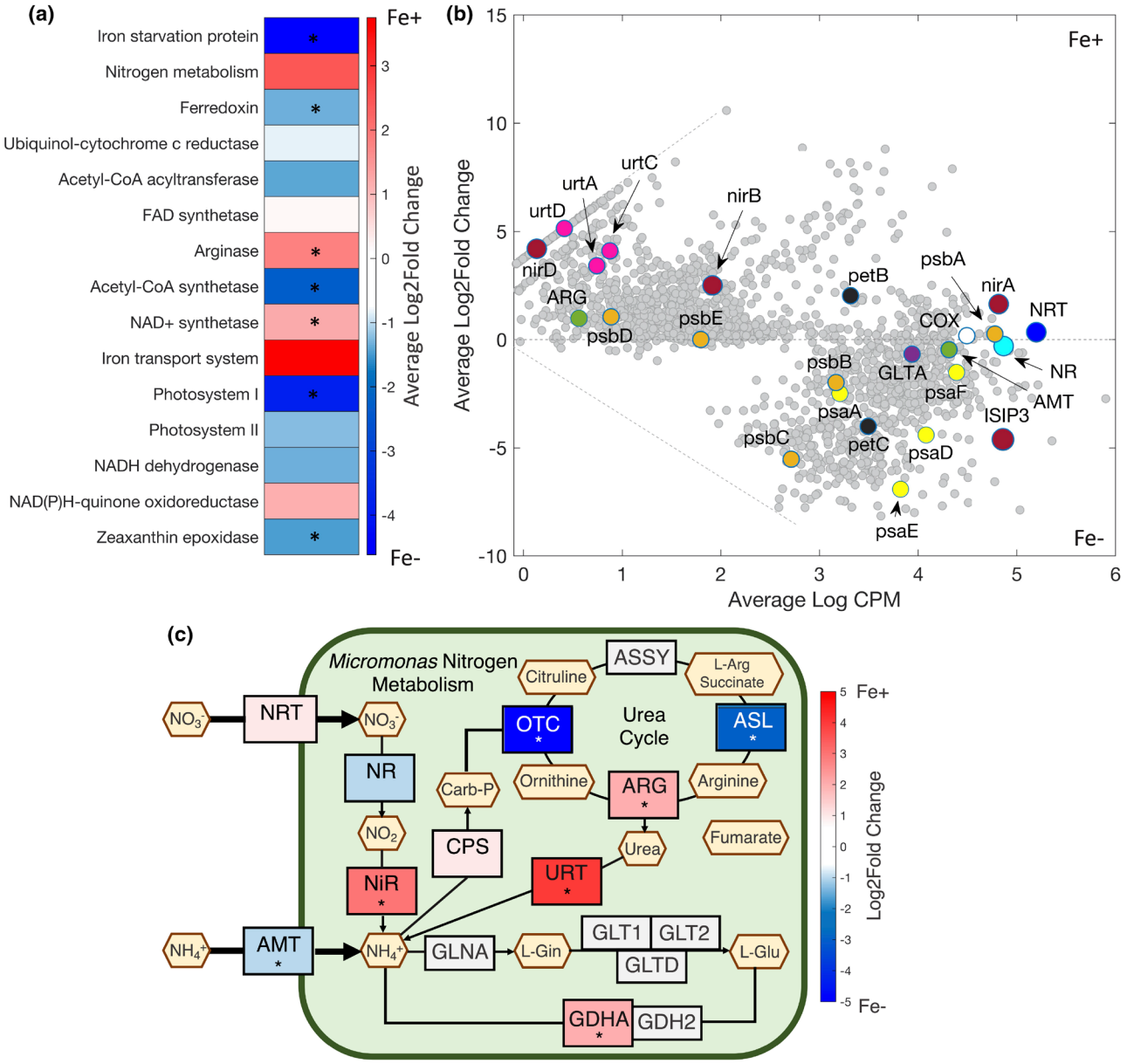

FIGURE 4 *Micromonas* sp. gene expression as a function of iron status. (a) Heatmap of average Log2Fold change (Fe+/Fe−) of KEGG pathways, (b) RA plot of average log counts per million (CPM) versus average Log2Fold change (Fe+/Fe−) of annotated contigs, and (c) Nitrogen assimilation pathway map of *Micromonas* sp. average Log2Fold change (Fe+/Fe−) of RNA transcripts. Transcripts were annotated and evaluated on the KO level using a significance threshold of $p < 0.05$. For all plots, positive Log2Fold change indicates overrepresentation in Fe+ cultures and negative Log2Fold change indicates overrepresentation in Fe− samples. Astericks on the heatmap and pathway map indicate significant changes ($p < 0.05$). The RA plot highlights protein-encoding genes of interest. The cellular pathway map indicates the sign and relative strength of Log2Fold change expression of genes. Gray genes are absent from transcript data. *NRT*, Nitrate transporter; *NiR*, nitrite reductase; *NR*, nitrate reductase; *AMT*, ammonium transporter; *OTC*, ornithine carbamolytransferase; *Urt*, urea transport; *Arg*, arginase; *Glta*, citrate synthase; *Psa*, photosystem I; *Psb*, photosystem II; *COX*, cytochrome c oxidase; *Pet*B, cytochrome b; *Pet*C, and cytochrome c.

diatoms, iron-replete *Micromonas* sp. were larger, had higher growth rates, had higher cellular Chl *a* content, and had appreciably higher C and N quotas relative to their iron-limited counterparts. Although the Fe-limited cells were smaller with lower growth rates and cellular quotas, they were able to reach higher cell densities under similar culturing conditions. These findings suggest *Micromonas* can achieve numerically dominance in iron-limited environments by reducing their cellular elemental quotas.

Iron-limitation strategies

Our results are in line with previous work (Boyd et al., 1998; Marchetti et al., 2006; Martin & Fitzwater, 1988),

suggesting low Fe concentrations limit nitrate uptake as is supported by a low relative growth rate (μ/μ_{max}). This leads to substantially curtailed growth rates and trends in gene expression where genes involved in nitrate metabolism (e.g., *NRT* and *NiR*) are more highly expressed under iron-replete conditions. The enhanced expression of genes related to nitrogen metabolism under iron replete conditions as well as our Fe+ modeled rates consistent with those small-celled new production rates measured during EXPORTS suggest that picoeukaryotes such as *Micromonas* may be important contributors to new production in the iron-limited waters of the Northeast Pacific. Our data also demonstrated clear expression patterns in genes involved in NO_3^- metabolism coinciding with their ability to grow effectively using NO_3^-.

Micromonas also appeared capable of urea metabolism by expressing urea transporters in addition to *NiR* and *NRT*. A similar finding was reported by Piganeau et al. (2011), who exhibited selective pressure for nitrate and urea uptake but not ammonium uptake. This finding is consistent with our inability to establish steady-state growth when cells were grown in NH_4^+-based media. However, this is surprising given the need to reduce NO_3^- to NH_4^+ for utilization in protein synthesis and the lower energetic cost of NH_4^+ utilization relative to NO_3^- utilization (Raven, 1988). Cultures were able to grow sporadically on NH_4^+, but steady-state growth was not achieved. This, combined with the presence of *AMT* in the transcriptome, supports previous studies (Cochlan & Harrison, 1991a, 1991b) and suggests *our Micromonas* isolate had the physiological capabilities for NH_4^+ utilization but were perhaps inhibited by some other factor, such as a vitamin or a micronutrient.

The lack of information on iron regulation was consistent with findings from previous studies of the closely related *Ostreococcus* (Lelandais et al., 2016; Sutak et al., 2012). The majority of what is known about marine phytoplankton iron metabolism comes from studies of diatoms (Marchetti et al., 2012; Peers & Price, 2006). It is, therefore, not surprising that many of the iron transport and homeostasis genes identified in diatoms were not readily identified in *Micromonas* given the substantial physiological differences between the two phytoplankton groups. The only iron-related gene identified and present in the *Micromonas* transcriptome was ISIP3, an iron-starvation induced protein with ferritin-like domains (Behnke & La Roche, 2020). However, similar to what was noted by Lelandais et al. (2016) for *Ostreococcus*, the high percentage of unannotated genes in our strain suggests that chlorophytes likely have novel methods for dealing with iron limitation that have not yet been well characterized. This idea was supported by lower identification of annotated genes with low transcript abundances associated with Fe-limited cells compared to Fe-replete cells (Figure 4b). Sutak et al. (2012) also observed that both *Ostreococcus* and *Micromonas* were able to take up ferric and ferrous iron without prior iron reduction but were unable to store it. The authors hypothesized ferritin may have be present in *Ostreococcus* but not in *Micromonas* (Sutak et al., 2012). Our study represents an analysis of *Micromonas* isolated from an HNLC region. The cosmopolitan nature and wide thermal niche of *Micromonas* suggests it can adapt to new or changing environments and proliferate quickly (Demory et al., 2019; Vannier et al., 2016). This may suggest the isolate studied here exhibits physiological characteristics and adaptations that may be quite different from what is currently characterized in the scientific literature using isolates from other regions.

An additional, noteworthy finding is that our data appears to suggest that *Micromonas* exhibit a form of nitrogen metabolism conservation even under Fe-replete conditions. The gene expression analysis demonstrates most protein-encoding genes related to nitrogen metabolism (*NRT*, *NR*, *AMT*, and *nir*A) have some of the highest constitutive transcript abundances of any pathway, exhibiting some significant directionality of gene expression under variable Fe conditions, but only to a minimal extent (Figure 4b). Some studies have suggested diatoms exhibit substantial changes in expression of genes involved in nitrogen metabolism, particularly in the natural environment (Marchetti et al., 2012), whereas others have likewise shown a lack of substantial change in gene expression (but not protein synthesis) in diatoms grown in culture (Cohen et al., 2018). These results support previous studies which have suggested picoeukaryotes and other small phytoplankton provide a "baseline" rate of primary production under limiting conditions with a minimal physiological response to dramatic shifts in environmental conditions (Meyer et al., 2022). It is possible that *Micromonas* expresses additional genomic adaptation strategies for iron limitation that were not identified from our transcriptome analysis. Additional research is needed to fully elucidate the strategies *Micromonas* uses to subsist in iron-limited environments.

Oceanographic context

Our study provides valuable cellular characteristics of an abundant picoeukaryote in a climatologically important oceanographic context. Meyer et al. (2022) observed that small cells (<5 μm) accounted for the majority of biomass (68% of total biomass) and primary production (89% of total primary production), including new production (72% of total new production), at Station P during the EXPORTS observation period. Furthermore, *Micromonas* appeared to be highly represented within the small-celled phytoplankton community, with 18S rDNA gene data indicating that *Micromonas* was within the top 20% of the most abundant phytoplankton genera and one of the top five most abundant picoeukaryotes (Jones & Rynearson, 2022). Although caution should be taken in

inferring cell abundance from 18S rDNA gene data alone, *Micromonas* has been shown to contain comparable gene copy numbers to other members of the Mamiellales order (Bachy et al., 2022; Zhu et al., 2005), and those numbers were observed to be on the low end compared to other phytoplankton groups (Gong & Marchetti, 2019). Combined with the flow cytometry data, this finding supports a high relative abundance of *Micromonas* and is thus not likely just a methodological caveat.

Our estimated rates of new production by picoeukaryotes such as *Micromonas*, which was taken as a representative species, under variable iron conditions were comparable to the average small-celled new production rates of $33.3 \pm 14.4\,\text{nmol}\,\text{N}\cdot\text{L}^{-1}\cdot\text{d}^{-1}$ from the North Pacific EXPORTS campaign (Figure 3). Although higher rates of NO_3^- uptake may occur within a culture relative to a mixed, natural phytoplankton community, our analysis supports the idea that *Micromonas* contributes substantially to total new production at Station P, especially when iron concentrations can support higher growth rates and cellular nitrogen quotas. Inherently, other phytoplankton groups, both within the picoplankton and nanoplankton size ranges, present at Station P during the EXPORTS observation period also contribute appreciably to new production. Our culture-based analysis is not meant to suggest *Micromonas* accounted for all of this new production; rather, this chlorophyte should at least be considered as a significant contributor to new production (and by inference, potentially to carbon export) as estimated from in situ picoeukaryote cell densities along with our measured cellular nitrogen quotas and growth rates as a function of iron status.

With projected decreases in euphotic zone nutrient concentrations in many parts of the oceans as a result of climate change (Kwiatkowski et al., 2020), accompanied by induced changes in water mass stratification and overall circulation, models of future projections predict an overall shift towards dominance by smaller phytoplankton groups such as chlorophytes (Henson et al., 2021). Abundant, small-cell phytoplankton with streamlined genomes and enhanced capabilities to adapt to changing environmental conditions such as *Micromonas,* hold distinct advantages in future climate conditions. Recent studies have suggested an ecological advantage for *Micromonas* in the Arctic where warmer temperatures and higher pCO_2 concentrations can induce higher rates of primary production (Hoppe et al., 2018). Further studies on *Micromonas* grazing rates, sinking speeds, and mixotrophic capabilities are needed to fully understand its ecology moving forward as well as how this will impact net carbon export rates and trophic level interactions.

CONCLUSIONS

In low-iron environments, *Micromonas* sp. exhibits physiological strategies, including reduced growth rates, small cell size, and metabolic restructuring, to combat Fe limitation and maintain high rates of new production and substantial abundances. This study furthers our understanding of this poorly characterized picoeukaryote and verifies a potential role for chlorophytes in performing new production in iron-limited regions. Here, we add to the body of knowledge reaffirming the need to shift our thinking on key phytoplankton groups that have the potential to contribute to carbon export and to pay additional attention to the role picoeukaryotes play in ecosystem dynamics both in current and future ocean climate scenarios.

AUTHOR CONTRIBUTIONS

Meredith G. Meyer: Conceptualization (equal); data curation (equal); formal analysis (equal); investigation (equal); methodology (equal); project administration (equal); resources (equal); software (equal); validation (equal); visualization (equal); writing – original draft (equal); writing – review and editing (equal). **Vincent J. White:** Data curation (equal); formal analysis (equal); methodology (equal); writing – original draft (equal). **Olivia Torano:** Data curation (equal); investigation (equal); writing – review and editing (equal). **Heidi Hannoush:** Data curation (equal); formal analysis (equal); methodology (equal); writing – original draft (equal). **Margarita Lankford:** Formal analysis (equal); writing – original draft (equal). **Adrian Marchetti:** Conceptualization (equal); data curation (equal); formal analysis (equal); funding acquisition (lead); investigation (equal); methodology (equal); project administration (equal); resources (equal); software (equal); supervision (lead); validation (equal); visualization (equal); writing – original draft (equal); writing – review and editing (equal).

ACKNOWLEDGMENTS

We thank the EXPORTS Chief Scientists, D. Steinberg and J. Graff, and the Captain and crew of the *R/V* Roger Revelle for their roles in the initial sample collection, R. Paerl for use of a flow cytometer, and J. Graff for NP EXPORTS flow cytometry data. We also thank R. Flynn and E. Speciale for helpful comments on the manuscript. This work was supported by NASA Grant 80NSSC17K0552 and NSF Grant OCE2219973 to AM.

DATA AVAILABILITY STATEMENT

All data presented here are publicly available at the National Center for Biotechnology Information (accession numbers within) and the Biological and Chemical Oceanography Data Management Office (project ID: 914269).

ORCID

Meredith G. Meyer https://orcid.org/0000-0002-9812-2908

REFERENCES

Andrew, S. M., Moreno, C. M., Plumb, K., Hassanzadeh, B., Gomez-Consarnau, L., Smith, S. N., Schofield, O., Fujiwara, T., Sunda, W. G., Hopkinson, B. M., Septer, A. N., & Marchetti, A. (2023). Widespread use of proton-pumping rhodopsin in Antarctic phytoplankton. *Proceedings of the National Academy of Science*, *120*(39), e2307638120. https://doi.org/10.1073/pnas.2307638120

Bachy, C., Sudek, L., Choi, C. J., Eckmann, C. A., Nothig, E.-M., Metfies, K., & Worden, A. Z. (2022). Phytoplankton surveys in the Arctic Fram Strait demonstrate the tiny eukaryotic alga *Micromonas* and other picoprasinophytes contribute to deep sea export. *Microorganisms*, *10*(5), 961. https://doi.org/10.3390/microorganisms10050961

Behnke, J., & La Roche, J. (2020). Iron uptake proteins in algae and the role of iron starvation-induced proteins (ISIPs). *European Journal of Phycology*, *55*(3), 339–360. https://doi.org/10.1080/09670262.2020.1744039

Boyd, P. W., Berges, J. A., & Harrison, P. J. (1998). In vitro enrichment experiments at iron-rich and -poor sites in the NE subarctic Pacific. *Journal of Experimental Marine Biology and Ecology*, *227*, 133–151. https://doi.org/10.3354/meps136179

Brand, L. E., Guillard, R. R. L., & Murphy, L. S. (1981). A method for rapid and precise determination of acclimated phytoplankton reproduction rates. *Journal of Plankton Research*, *3*(2), 193–201. https://doi.org/10.1093/plankt/3.2.193

Chisholm, S. W., Frankel, S. L., Goericke, R., Olson, R. J., Palenik, B., Waterbury, J. B., West-Johnsrud, L., & Zettler, E. R. (1991). *Prochlorococcus marinus* nov. gen. nov. sp.: An oxyphototrophic marine prokaryote containing divinyl chlorophyll *a* and *b*. *Archives of Microbiology*, *157*, 297–300.

Cochlan, W. P., & Harrison, P. J. (1991a). Uptake of nitrate, ammonium, and urea by nitrogen-starved cultures of *Micromonas pusilla* (Prasinophyceae): Transient responses. *Journal of Phycology*, *27*, 673–679.

Cochlan, W. P., & Harrison, P. J. (1991b). Kinetics of nitrogen (nitrate, ammonium and urea) uptake by the picoflagellate *Micromonas pusilla* (Prasinophyceae). *Journal of Experimental Marine Biology and Ecology*, *153*, 129–141.

Cohen, N. R., Gong, W., Moran, D. M., McIlvin, M. R., Saito, M. A., & Marchetti, A. (2018). Transcriptomic and proteomic responses of the oceanic diatom *Pseudo-nitzschia granii* to iron limitation. *Environmental Microbiology*, *20*(8), 3109–3126. https://doi.org/10.1111/1462-2920.15386

Demory, D., Baudoux, A.-C., Monier, A., Simon, N., Six, C., Ge, P., Rigaut-Jalabert, F., Marie, D., Sciandra, A., Bernard, O., & Rabouille, S. (2019). Picoeukaryotes of the *Micromonas* genus: Sentinels of a warming ocean. *The ISME Journal*, *13*, 132–146. https://doi.org/10.1038/s41396-018-0248-0

Ellis, K. (2015). *The coeffects of iron and vitamin B12 on marine diatoms* [Master's thesis, University of North Carolina at Chapel Hill]. UNC Carolina Digital Repository. https://doi.org/10.17615/sjm6-0c93 .

Fowler, B. L., Neubert, M. G., Hunter-Cevera, K. R., Olson, R. J., Shalapyonok, A., Solow, A. R., & Sosik, H. (2020). Dynamics and functional diversity of the smallest phytoplankton on the Northeast US Shelf. *Proceedings of the National Academy of Science*, *117*(22), 12215–12221. https://doi.org/10.1073/pnas.1918439117

Fu, L., Beifang, N., Zhu, Z., Wu, S., & Weizhong, L. (2012). CD-HIT: Accelerated for clustering the next-generation sequencing data. *Bioinformatics*, *28*(23), 3150–3152. https://doi.org/10.1093/bioinformatics/bts565

Gong, W., & Marchetti, A. (2019). Estimation of 18S gene copy number in marine eukaryotic plankton using a next-generation sequencing approach. *Frontiers of Marine Science*, *6*, 219. https://doi.org/10.3389/fmars.2019.00219

Gorbunov, M. Y., & Falkowski, P. G. (2004). Fluorescence induction and relaxation (FIRe) technique and instrumentation for monitoring photosynthetic processes and primary production in aquatic ecosystems. In A. Van Der Est, & D. Bruce (Eds.), *Photosynthesis: Fundamental Aspects to Global Perspectives* (pp. 1029–1031). Alliance Communications Group.

Graff, J. R. (2023). *Data from the EXport processes in the ocean from remote sensing North Pacific campaign (Version 1)*. NASA SeaWiFS Bio-optical Archive and Storage System (SeaBASS). https://oceandata.sci.gsfc.nasa.gov/ob/getfile/f092f8f02a_EXPORTS_EXPORTSNP_RR1813_Graff_Cphyto_Analytical_R0.sb

Graff, J. R., & Rynearson, T. A. (2011). Extraction method influences the recovery of phytoplankton pigments from natural assemblages. *Limnology and Oceanography*, *9*, 129–139. https://doi.org/10.4319/lom.2011.9.129

Greene, R. M., Geider, R. J., Kolber, Z., & Falkowski, P. G. (1992). Iron-induced changes in light harvesting and photochemical energy conversion processes in eukaryotic marine algae. *Plant Physiology*, *100*, 565–575. https://doi.org/10.1104/pp.100.2.565

Henson, S. A., Cael, B. B., Allen, S. R., & Dutkiewicz, S. (2021). Future phytoplankton diversity in a changing climate. *Nature Communications*, *12*, 5372. https://doi.org/10.1038/s41467-021-25699-w

Hoppe, C. J. M., Flintrop, C. M., & Rost, B. (2018). The Arctic picoeukaryote *Micromonas pusilla* benefits synergistically from warming and ocean acidification. *Biogeosciences*, *15*, 4353–4365. https://doi.org/10.5194/bg-15-4353-2018

Jones, E., & Rynearson, T. (2022). *Data from the EXport processes in the ocean from RemoTe sensing North Pacific campaign (Version 1)*. National Center for Biotechnology Information (NCBI). https://www.ncbi.nlm.nih.gov/bioproject/796004

Kwiatkowski, L., Torres, O., Bopp, L., Aumont, O., Chamberlain, M., Christian, J. R., Dunne, J. P., Gehlen, M., Ilyina, T., John, J. G., Lenton, A., Li, H., Lovenduski, N. S., Orr, J. C., Palmieri, J., Santana-Falcon, Y., Schwinger, J., Seferian, R., Stock, C. A., … Ziehn, T. (2020). Twenty-first century ocean warming, acidification, deoxygenation, and upper-ocean nutrient and primary production decline from CMIP6 model projections. *Biogeosciences*, *17*(13), 3439–3470. https://doi.org/10.5194/bg-17-3439-2020

La Roche, J., Geider, R. J., Graziano, L. M., Murray, H., & Lewis, K. (1993). Induction of specific proteins in eukaryotic algae grown under iron-, phosphorus-, or nitrogen-deficient conditions. *Journal of Phycology*, *29*, 767–777. https://doi.org/10.1111/j.0022-3646.1993.00767.x

Le Gall, F., Rigaut-Jalabert, F., Marie, D., Garczarek, L., Viprey, M., Gobet, A., & Vaulot, D. (2008). Picoplankton diversity in the South-East Pacific Ocean from cultures. *Biogeosciences*, *5*, 203–214. https://doi.org/10.5194/bg-5-203-2008

Lelandais, G., Scheiber, I., Paz-Yepes, J., Lozano, J., Botebol, H., Pilatova, J., Zarsky, V., Leger, T., Blaiseau, P., Bowler, C., Bouget, F., Camadro, J., Sutak, R., & Lesuisse, E. (2016). *Ostreococcus tauri* is a new model green alga for studying iron metabolism in eukaryotic phytoplankton. *BMC Genomics*, *17*, 319. https://doi.org/10.1186/s12864-016-2666-6

Marchetti, A., Juneau, P., Whitney, F. A., Wong, C., & Harrison, P. J. (2006). Phytoplankton processes during a mesoscale iron enrichment in the NE subarctic Pacific: Part II- nutrient utilization. *Deep Sea Research, Part II*, *53*, 2114–2130. https://doi.org/10.1016/j.dsr2.2006.05.038

Marchetti, A., Parker, M. S., Moccia, L. P., Lin, E. O., Arrieta, A. L., Ribalet, F., Murphy, M. E. P., Maldonado, M. T., & Armbrust, E. V. (2009). Ferritin is used for iron storage in bloom-forming marine pennate diatoms. *Nature*, *457*, 467–470. https://doi.org/10.1038/nature07539

Marchetti, A., Schruth, D. M., Durkin, C. A., Parker, M. S., Kodner, R. B., Berthiaume, C. T., Morales, R., Allen, A. E., & Armbrust, E. V. (2012). Comparative metatranscriptomics identifies molecular bases for the physiological responses of phytoplankton to varying iron availability. *Proceedings of the National Academy*

of Sciences, *109*(6), E317–E325. https://doi.org/10.1073/pnas.1118408109
Martin, J. H., & Fitzwater, S. (1988). Iron deficiency limits phytoplankton growth in the north-east Pacific subarctic. *Nature*, *331*, 341–343. https://doi.org/10.1038/331341a0
McKie-Krisberg, Z. M., & Sanders, R. W. (2014). Phagotrohy by the picoeukaryotic green alga Micromonas: implications for Arctic Oceans. *The ISME Journal*, *8*(10), 1953–1961. https://doi.org/10.1038/ismej.2014.16
Meyer, M. G., Gong, W., Kafrissen, S. M., Torano, O., Varela, D. E., Santoro, A. E., Cassar, N., Gifford, S., Niebergall, A. K., Sharpe, G., & Marchetti, A. (2022). Phytoplankton size-class contributions to new and regenerated production during the EXPORTS Northeast Pacific Ocean field deployment. *Elementa: Science of the Anthropocene*, *10*, 68. https://doi.org/10.1525/elementa.2021.00068
Monier, A., Worden, A. Z., & Richards, T. A. (2016). Phylogenetic diversity and biogeography of the Mamiellophyceae lineage of eukaryotic phytoplankton across the oceans. *Environmental Microbiology Reports*, *8*(4), 461–469. https://doi.org/10.1111/1758-2229.12390
Moore, L. R., Post, A. F., Rocap, G., & Chisholm, S. W. (2002). Utilization of different nitrogen sources by the marine cyanobacteria, *Prochlorococcus* and *Synechococcus*. *Limnology and Oceanography*, *47*(4), 989–996.
Moreno, C. M., Gong, W., Cohen, N. R., DeLong, K., & Marchetti, A. (2020). Interactive effects of iron and light limitation on the molecular physiology of the Southern Ocean diatom *Fragilariopsis kerguelensis*. *Limnology and Oceanography*, *65*(7), 1511–1531. https://doi.org/10.1002/lno.11404
Moreno, C. M., Lin, Y., Davies, S., Monbureau, E., Cassar, N., & Marchetti, A. (2017). Examination of gene repertoires and physiological responses to iron and light limitation in Southern Ocean diatoms. *Polar Biology*, *41*, 679–696. https://doi.org/10.1007/s00300-017-2228-7
Paerl, R. W., Venezia, R. E., Sanchez, J. J., & Paerl, H. W. (2020). Picophytoplankton dynamics in a large temperate estuary and impacts of extreme storm events. *Scientific Reports*, *10*, 22026. https://doi.org/10.1038/s41598-020-79157-6
Patro, R., Duggal, G., Love, M. I., Irizarry, R. A., & Kingsford, C. (2017). Salmon provides fast and bias-aware quantification of transcript expression. *Nature Methods*, *14*, 417–419.
Peers, G., & Price, N. M. (2006). Copper-containing plastocyanin used for electron transport by an oceanic diatom. *Nature*, *441*, 341–344. https://doi.org/10.1038/nature04630
Piganeau, G., Grimsley, N., & Moreau, H. (2011). Genome diversity in the smallest marine photosynthetic eukaryotes. *Research in Microbiology*, *162*(6), 570–577. https://doi.org/10.1016/j.resmic.2011.04.005
Price, N. M., Ahner, B. A., & Morel, F. M. M. (1994). The equatorial Pacific Ocean: Grazer-controlled phytoplankton populations in an iron-limited ecosystem. *Limnology and Oceanography*, *39*, 520–534. https://doi.org/10.4319/lo.1994.39.3.0520
Price, N. M., Harrison, G. I., Hering, J. G., Hudson, R. J., Nirel, P. M. V., Palenik, B., & Morel, F. M. M. (1989). Preparation and chemistry of the artificial algal culture medium Aquil. *Biological Oceanography*, *6*, 443–461. https://doi.org/10.1080/10965581.1988.10749544
Raven, J. A. (1988). The iron and molybdenum use efficiencies of plant growth with different energy, carbon, and nitrogen sources. *New Phytologist*, *109*, 279–287. https://doi.org/10.1111/j.1469-8137.1988.tb04196.x
Sharpe, G., Zhao, L., Meyer, M. G., Gong, W., Burns, S. M., Tagliabue, A., Buck, K. N., Santoro, A. E., Graff, J. R., Marchetti, A., & Gifford, S. (2023). *Synechococcus* nitrogen gene loss in iron-limited ocean regions. *ISME Communications*, *3*, 107. https://doi.org/10.1038/s43705-023-00314-9
Soneson, C., Love, M. I., & Robinson, M. D. (2015). Differential analyses for RNA-seq: Transcript-level estimates improve gene-level inferences. *F1000Research*, *4*, 1521. https://doi.org/10.12688/f1000research.7563.1
Sutak, R., Botebol, H., Blaiseau, P.-L., Leger, T., Bouget, F.-Y., Camadro, J.-M., & Lesuisse, E. (2012). A comparative study of iron uptake mechanisms in marine microalgae: Iron binding at the cell surface is a critical step. *Plant Physiology*, *160*, 2271–2284. https://doi.org/10.1104/pp.112.204156
Vannier, T., Leconte, J., Seeleuthner, Y., Mondy, S., Pelletier, E., Aury, J., de Vargas, C., Sierack, M., Iudicone, D., Vaulot, D., Wincker, P., & Jaillon, O. (2016). Survey of the green picoalga *Bathycoccus* genomes in the global ocean. *Scientific Reports*, *6*, 37900. https://doi.org/10.1038/srep37900
Varela, D. E., & Harrison, P. J. (1999). Seasonal variability in nitrogenous nutrition of phytoplankton assemblages in the northeastern subarctic Pacific Ocean. *Deep Sea Research Part II: Topical Studies in Oceanography*, *46*, 2505–2538. https://doi.org/10.1016/S0967-0645(99)00074-0
Worden, A. Z., & Not, F. (2008). Ecology and diversity of picoeukaryotes. *Microbial Ecology of the Oceans*, *2*, 159–205.
Zhu, F., Massana, R., Not, F., Marie, D., & Vaulot, D. (2005). Mapping of picoeucaryotes in marine ecosystems with quantitative PCR of the 18S rRNA gene. *Microbiology Ecology*, *52*(1), 79–92. https://doi.org/10.1016/j.femsec.2004.10.006

SUPPORTING INFORMATION

Additional supporting information can be found online in the Supporting Information section at the end of this article.

Figure S1. Flow cytometry cytograms from (a) the North Pacific EXPORTS cruise, (b) NO_3^- Fe− samples, and (c) NO_3^- Fe+ samples. On panel A, the axes represent forward scatter (FSC) and side scatter (SSC) whereas on panels B and C, the axes represent forward scatter (FSC) and red fluorescence. The dashed box on panel A indicates the FSC gated regions (red shapes) for the culture samples.

Figure S2. Schematic flow chart of metatranscriptomic/transcriptomic sample processing. Key steps are outlined in boxes and associated software, references, databases, etc. are located next to each step. ISIP denotes Iron Starvation Induced Protein. Further information on code can be found at github.com/omtorano/Exports-Metatranscriptomics/.

Table S1. Statistical tests for significant differences of growth rates, maximum photochemical yield of PSII (F_v/F_m), cell volume, chlorophyll *a* concentrations, carbon quotas and nitrogen quotas, C:N ratios and C:Chl *a* ratios from paired two-tailed *t*-tests between Fe− and Fe+ treatments. All three replicates in the Fe− and Fe+ treatments were included for the statistical analyses.

How to cite this article: Meyer, M. G., White, V. J., Torano, O., Hannoush, H., Lankford, M., & Marchetti, A. (2025). The effects of iron limitation on the small chlorophyte *Micromonas* from the Northeast Pacific Ocean. *Journal of Phycology*, *00*, 1–12. https://doi.org/10.1111/jpy.70079